J. Plasma Phys. (2025), *vol*. 91, E107
 doi:10.1017/S0022377825100445

The impact of intrinsic magnetisation and Ohmic diffusion on Jeans instability in strongly magnetised anisotropic quantum plasmas

Vinesh Kumar Sangwan[1], Ravinder Bhambhu[1] and Ram Prasad Prajapati[1]

[1]School of Physical Sciences, Jawaharlal Nehru University, New Delhi 110067, India

Corresponding author: Ram Prasad Prajapati, rpprajapati@mail.jnu.ac.in

(Received 21 December 2024; revision received 12 May 2025; accepted 12 May 2025)

We have investigated the modified Jeans instability and gravitational collapse in uniformly rotating, anisotropic quantum plasmas, including the effects of intrinsic magnetisation, viscosity tensor and Ohmic diffusivity. The closure of the Chew, Goldberger and Low and quantum magnetohydrodynamic fluid models describes the dynamical properties and modified dispersion characteristics of the system. The modified Jeans instability criteria and Jeans wavenumbers for the onset conditions of gravitational collapse are obtained, which are significantly modified due to spin magnetisation, quantum corrections and rotation of the system. Strong magnetisation and electrical resistivity are found to enhance the growth rate of Jeans instability, making the system more gravitationally unstable. The magnetic field shows both stabilising (in weak magnetisation limit) and destabilising (in strong magnetisation limit) influence on the growth rate by affecting the gravitational collapse mechanism of dense stars. The growth rate of pressure-anisotropy-driven firehose instability is destabilised due to pressure anisotropy, rotation and spin magnetisation effects. The results are discussed in order to understand the Jeans instability and gravitational collapse of low-mass strongly magnetised white dwarfs.

Key words: astrophysical plasmas, plasma instabilities, quantum plasma

1. Introduction

The interior of highly magnetised dense stars (e.g. white dwarfs, neutron stars and magnetars) exhibits distinct properties due to the existence of degenerate particles in the quantum regime at extremely low temperatures ($T < T_F$, where T_F is the Fermi temperature). The quantum effects become unavoidable and play a vital role in dense plasmas when the de Broglie wavelength of the plasma species is comparable to or larger than their interparticle separation, i.e. $\lambda_B \geqslant n_0^{-1/3}$ (where n_0 is the average particle density) (Bonitz *et al*. 2010). The aforementioned condition is satisfied in magnetars ($\lambda_B \simeq 9 \times 10^{-13}$ m) and white dwarfs ($\lambda_B \simeq 3 \times 10^{-10}$ m) in which the orders of de Broglie wavelengths are equivalent to the interparticle separations in these systems (Gómez & Kandus 2018). The quantum mechanical behaviour of plasma particles is significant and has been notably studied in white dwarfs,

neutron stars, pulsars and magnetars, giant planets and laser fusion experiments (Chabrier 1993; Karpiuk *et al*. 2021). Quantum effects also play an unavoidable role in plasma screening for thermonuclear fusion in high-density laser experiments (Elsing, Pálffy & Wu 2022). In semiconductor plasmas, quantum effects are crucial in modifying instabilities, e.g. drift and modulation instabilities (Sharma *et al*. 2024). In past years, many fluid instabilities have been studied in quantum plasmas, such as filamentation instability (Bret 2007), magnetorotational instability (Usman & Mushtaq 2021), oblique waveguide instability (Jamil *et al*. 2020), electromagnetic instability (Khodadadi Azadboni 2021) and temperature-anisotropy-driven Weibel instability (Haas 2008). In addition, the Jeans instability is the fundamental mechanism in the formation of dense stars through gravitational collapse, which has been previously studied assuming the plasma pressure to be isotropic in nature (Shukla & Stenflo 2006).

In most quantum plasma systems, the spins of the constituent particles are randomly oriented; hence, the impact arising from spin-induced magnetisation can be safely ignored. Strong magnetic fields are present in dense stars, e.g. in white dwarfs ($B \simeq 10^6 - 10^9$ G) and neutron stars ($B \simeq 10^{12}$ G) (Wickramasinghe & Ferrario 2005). Further, in magnetars, there exists an ultra-strong magnetic field ($B \simeq 10^{14} - 10^{15}$ G) that exceeds the quantum critical threshold, $B_{\rm cr} = 4.4 \times 10^{13}$ G (Duncan & Thompson 1992). These strong magnetic fields are mainly responsible for magnetisation and affect the particle dynamics in degenerate plasmas. Strong magnetic fields also cause Landau quantisation in magnetars, which produces axion (Maruyama *et al*. 2018). These effects become significant in highly magnetised dense stars when the spin is aligned along the magnetic field (Brodin & Marklund 2007*a*). Spin magnetisation plays a crucial role via coupling to the Alfvénic speed by modifying the instability criteria and affecting the gravitational collapse in compact astrophysical objects (Usman, Mushtaq & Jan 2018). Spin forces are important even when their magnitudes are smaller than the usual $\boldsymbol{J} \times \boldsymbol{B}$ force, and this property is demonstrated by studying the one-dimensional nonlinear shear Alfvén waves (Brodin & Marklund 2007*b*). The propagation of the magnetosonic waves is affected by quantum corrections, such as the Bohm potential and the spin of the electron. The magnetohydrodynamics (MHD) formalism is used to analyse the normal modes in magnetised quantum plasmas with spin coupling, Fermi pressure and Hall effect (Gómez & Kandus 2018). Furthermore, the effects of spin magnetisation in quantum plasmas have been investigated in the study of nonlinear magnetosonic waves (Mushtaq & Vladimirov 2011), nonlinear Alfvén waves (Jan, Mushtaq & Ikram 2018) and magnetorotational instability (Usman & Mushtaq 2021). The growth rate of Weibel instability in strongly coupled quantum plasmas decreases due to the quantum parameter and increases due to the temperature anisotropy parameter (Nejadtaghi *et al*. 2024).

Analytical techniques have been developed to model quantum plasmas and investigate waves and instabilities. These are the Wigner–Poisson, Schrödinger–Poisson and quantum magnetohydrodynamic (QMHD) models (Haas 2005, 2011). The QMHD model is most appropriate for studying the macroscopic transport properties of a quantum fluid involving global plasma parameters. The properties of dense white dwarfs and neutron stars provide insightful predictions regarding their unique characteristics. The behaviour of relativistic degenerate electrons and exchange-correlation effects is studied on the propagation of high-frequency surface waves in spin-1/2 quantum plasmas and it has been shown that due to exchange-correlation effects, the frequency spectrum of high-frequency surface waves is shifted down (Chen *et al*. 2020). The ion-acoustic solitary waves in an electron–positron–ion

https://doi.org/10.1017/S0022377825100445 Published online by Cambridge University Press

quantum plasma in the presence of an external static magnetic field have been studied using the reductive perturbation method (El-Taibany *et al*. 2022). In the QMHD framework, dust magnetosonic waves are investigated in degenerate quantum plasmas, including spin and exchange-correlation effects (Maroof, Mushtaq & Qamar 2016). Rahim, Adnan & Qamar (2019) used the QMHD model to analyse the properties of small-amplitude magnetosonic shock waves in a dissipative plasma, including spin-up and spin-down electrons. In addition, many interesting phenomena, such as unstable charge density waves (Han, Zhang & Dai 2019) and nucleus-acoustic shock waves (Mamun, Sharmin & Tamanna 2021), show the importance of quantum effects in collective modes in low-temperature and highly dense plasmas. Recently, the dispersion properties of electron plasma waves in a nonlinear quantum plasma have been studied by applying the Volkov approach in the kinetic framework (Haas, Mendonça & Terças 2023).

Dense stars are formed due to the collapse of massive stars in which electron degeneracy pressure (in white dwarfs) and neutron degeneracy pressure (in neutron stars) support them against gravitational collapse (Leung 1985). The magnetic field has a unique role in the gravitational collapse of dense stars. In past years, many researchers have extended the problems of Jeans (gravitational) instability of quantum plasmas considering various physical effects in the environment of dense stars. Shukla & Stenflo (2006) have investigated the Jeans instabilities of self-gravitating astrophysical quantum dusty plasma assuming electrostatic perturbations. The QMHD model is used to analyse the Jeans instability in quantum plasmas considering the effects of finite Larmor radius corrections (Joshi *et al*. 2018), neutrino beam and flavour oscillations (Prajapati 2017; Hammad *et al*. 2023) and Fermi temperature ratio (Ali & Mushtaq 2011). Lundin, Marklund & Brodin (2008) have investigated the modified Jeans instability considering the spin magnetisation effect and found that it enhances the growth rate of the Jeans instability. However, the plasma pressure in dense highly magnetised astrophysical systems does not remain isotropic, and it becomes anisotropic in nature. Pressure-anisotropy-driven kinetic instabilities have recently been studied in magnetised low-density plasmas in the intracluster medium (Rappaz & Schober 2024). We find that none of these authors (Lundin *et al*. 2008; Gómez & Kandus 2018; Bhakta & Prajapati 2018; Sangwan & Prajapati 2023) have studied the role of intrinsic magnetisation, rotation, Ohmic diffusion and viscous dissipation in the Jeans instability in anisotropic quantum plasmas.

This paper analyses the influence of spin magnetisation, rotation, Ohmic diffusion and viscosity stress tensor on the Jeans instability in anisotropic quantum plasmas. The remaining part of the paper is organised as follows. In § 2, the anisotropic quantum fluid model is constructed using the Chew, Goldberger and Low (CGL) and QMHD fluid models for anisotropic quantum plasmas. In § 3, the dispersion relation of the modified Jeans instability is analytically derived by solving linearised perturbation equations and using the normal-mode method. In § 4, the general dispersion relation is analysed in the transverse and longitudinal modes to examine the role of spin magnetisation and other parameters. The applications of the analytical results for dense quantum plasmas in white dwarfs are discussed. Finally, the paper is summarised and concluded in § 5.

2. Anisotropic quantum fluid model

Let us discuss the gravitational collapse and Jeans instability in a highly dense, magnetised white dwarf consisting of pressure anisotropy ($p_{\parallel} \neq p_{\perp}$, where $p_{\parallel,\perp}$ are

https://doi.org/10.1017/S0022377825100445 Published online by Cambridge University Press

the pressure components parallel and perpendicular to the direction of the magnetic field) and viscosity tensor in finitely conducting quantum fluid. The plasma is embedded in the strong uniform magnetic field along the z axis, i.e. $\boldsymbol{B}(0, 0, B)$. Non-magnetic white dwarfs are generally slow rotators, having periods varying from a few days to a few hours. However, there are some white dwarfs, e.g. EUVE J0317-853, which are highly magnetised and rapidly rotating ($r_p = 700\,\mathrm{s}$) (Ferrario & Wickramasinghe 2005). Also, the plasma rotation on the surface of white dwarfs is less significant than the rigid rotation of these stars. Therefore, it is necessary to consider the rotation effects for such dense stars in the dynamical descriptions during the structure formation. It is assumed that the system is rotating along the z axis with uniform rotational frequency $\boldsymbol{\Omega}(0, 0, \Omega)$, which gives rise to the Coriolis force in the momentum transfer equation. Furthermore, the dynamics of plasma particles in white dwarfs may be relativistic or non-relativistic depending upon the size and mass of the star. In low-mass white dwarfs, ultra-relativistic degenerate electrons satisfy the equation of state $P \propto \rho^{4/3}$. On the other hand, non-relativistic degenerate electrons satisfy the equation of state $P \propto \rho^{5/3}$. In the present work, we deal with anisotropic pressure plasmas; thus the usual CGL fluid equations are considered following the work of Shukla & Stenflo (2008).

We also assume that the interior properties of the system consist of quantum plasmas with temperature (T) less than the Fermi temperature (T_F) so that the quantum effects become significant in the system, i.e.

$$T < T_F \equiv \frac{E_F}{k_B} = \frac{\hbar^2}{2mk_B}(3\pi^2)^{2/3} n_0^{2/3}, \tag{2.1}$$

where E_F, k_B and m are the Fermi energy, the Boltzmann constant and the mass of the particle, respectively.

The ratio $\xi = T_F/T$ signifies the behaviour of the system, and when $\xi \geqslant 1$ the quantum effects dominate in the system (Manfredi, Hervieux & Hurst 2021). The Fermi temperature is directly proportional to the number density, suggesting a high value of the Fermi temperature inside white dwarfs due to the high values of number densities. The quantum coupling parameter, which is basically the ratio of interaction energy to the Fermi energy, i.e. $\Gamma_Q \sim 1/(n\lambda_F^3)^{2/3} \sim (\hbar\omega_p/E_F)^2$ (where $\hbar\omega_p$ is the plasmon energy), is considered to be small in the collisionless regime (where collective and mean-field effects dominate). Plasmas with high densities are more collective because of Pauli's exclusion principle.

The quantum effects in the QMHD model appear through the Bohm potential term and intrinsic magnetisation effects. The quantum Bohm potential accounts for quantum effects like diffraction and quantum tunnelling, while the Fermi pressure represents the statistical pressures of the degenerate particles. In semiconductor physics, the Bohm potential is mainly responsible for tunnelling and differential resistance effects. The quantum Bohm force originates from interpreting a Fermi gas within the framework of hidden variables in quantum mechanics (Bohm 1952) which is given by

$$\boldsymbol{F_Q} = \frac{\hbar^2}{2m_e}\nabla\left(\frac{\nabla^2\sqrt{n_e}}{\sqrt{n_e}}\right), \tag{2.2}$$

where m_e is the electron mass and n_e is the electron number density.

The QMHD equations for dense magnetoplasma, including electron temperature anisotropy, are derived by Shukla & Stenflo (2008) in the MHD limit. In previous

https://doi.org/10.1017/S0022377825100445 Published online by Cambridge University Press

works (Lundin *et al*. 2008; Modestov, Bychkov & Marklund 2009), authors have separately studied the effects of quantum Bohm potential, spin magnetisation and self-gravitation using the QMHD fluid model of Haas (2005). The MHD instability and Jeans instability in viscous resistive quantum plasma are studied considering the spin magnetisation terms in the equation of motion (Bychkov, Modestov & Marklund 2010; Sharma & Chhajlani 2014). Gómez & Kandus (2018) have also formulated a two-fluid QMHD model considering spin–magnetic coupling irrespective of all other spin interactions. However, the theory of spin magnetisation in dense plasmas and QMHD equations is still a grey area of research owing to their limitations in real physical systems (Bonitz, Moldabekov & Ramazanov 2019). We suggest the validity of this theory in the core of white dwarfs, where iron is present in abundance. The ferromagnetic properties of iron make the spin magnetisation effect important while studying the gravitational collapse of dense quantum plasmas in the core of white dwarfs.

The strong correlation between plasma constituents in dense stars originates from the Coulomb force, quantum degeneracy and magnetic confinement, enhanced by extreme density and magnetic fields. These conditions create a highly organised plasma state in which electrons and ions cannot behave independently, especially when external magnetic fields impose additional constraints on motion and interactions. Additionally, in the framework of the spin-magnetised quantum plasma, spin alignment along the magnetic field contributes to the magnetisation of the system, further enhancing inter-particle correlations. This spin-induced magnetisation modifies the collective behaviour of the plasma and alters the propagation of low-frequency modes such as those associated with Jeans and firehose instabilities.

Therefore, considering the strong correlations between plasma constituents due to the aforementioned effects, we write the single fluid equation of motion as (Haas 2005; Brodin & Marklund 2007*a*; Lundin *et al*. 2008; Bychkov *et al*. 2010)

$$\rho\left(\frac{\partial}{\partial t}+\boldsymbol{V}\cdot\nabla\right)\boldsymbol{V}=-\nabla\cdot\overleftrightarrow{\boldsymbol{P}}-\nabla\cdot\overleftrightarrow{\boldsymbol{\Pi}}-\rho\nabla\phi_g+2\rho(\boldsymbol{V}\times\boldsymbol{\Omega})-\nabla\left(\frac{B^2}{2\mu_0}-\boldsymbol{M}\cdot\boldsymbol{B}\right)+\boldsymbol{B}\cdot\nabla\left(\frac{\boldsymbol{B}}{\mu_0}-\boldsymbol{M}\right)+\frac{\hbar^2\rho}{2m_e m_i}\nabla\left(\frac{\nabla^2\sqrt{\rho}}{\sqrt{\rho}}\right). \tag{2.3}$$

The continuity equation is

$$\frac{\partial\rho}{\partial t}+\nabla\cdot(\rho\boldsymbol{V})=0, \tag{2.4}$$

where $\boldsymbol{V}$, $\overleftrightarrow{\boldsymbol{P}}$, $\boldsymbol{B}$, ϕ_g, $\overleftrightarrow{\boldsymbol{\Pi}}$, ρ and $\boldsymbol{M}$ are the fluid velocity, the pressure tensor, the magnetic field vector, the gravitational potential, the viscosity tensor, the quantum fluid density and the magnetisation due to electron spin, respectively.

On the right-hand side of (2.3), many force terms appear that describe the dynamics of the considered plasma configuration. The inclusion of additional force terms in the basic QMHD model of Haas (2008) extensively describes the wave modes and instabilities in quantum plasmas, as many researchers have discussed (Lundin *et al*. 2008; Asenjo 2012; Sharma & Chhajlani 2013; Rahim *et al*. 2019). The first two terms, respectively, show the anisotropic pressure tensor and viscosity stress tensor. Since large masses are involved in white dwarfs, the self-gravitational force term becomes unavoidable and is included as the gradient of a scalar potential ϕ_g.

https://doi.org/10.1017/S0022377825100445 Published online by Cambridge University Press

The quantum effects are included in terms of Bohm potential as derived in the QMHD model (Haas 2005) and spin magnetisation due to the interaction between the magnetic field $\boldsymbol{B}$ and magnetisation vector $\boldsymbol{M}$ (Brodin & Marklund 2007*a*; Modestov *et al*. 2009). The fourth term represents the centrifugal force, which shows the rotation of the system.

The dynamics is considered on a time scale larger than the inverse cyclotron frequency but shorter than the inverse spin transition frequency, so that the effects of spin-flip do not occur, which happens because of particle collisions and also due to the time variation of the magnetic field. The temporal variation of the magnetic field should be smaller than the inverse cyclotron frequency of the electron (Brodin, Marklund & Manfredi 2008). In this case, the magnetisation vector is given by (Brodin & Marklund 2007*a*; Lundin *et al*. 2008)

$$\boldsymbol{M} = \frac{\mu_B \rho}{m_i} \tanh\left(\frac{\mu_B B}{k_B T}\right) \hat{\boldsymbol{B}}, \tag{2.5}$$

where μ_B is the Bohr magnetron and m_i is the mass of ions. The factor $\tanh(\mu_B B/k_B T)$ appears by virtue of the fact that the spin vector is aligned parallel to the magnetic field and the system reaches the thermodynamic equilibrium state. Generally, the spin is randomly oriented for most plasmas, so the factor $\mu_B B/k_B T$ is very small, and the spin quantum effects are negligible. Meanwhile, the spin effects are significant in low-frequency wave motions for plasmas that are highly magnetised or have low temperatures (Marklund & Brodin 2007).

The magnetic field equations using the modified Ohm's law are

$$\frac{\partial \boldsymbol{B}}{\partial t} = \boldsymbol{\nabla} \times (\boldsymbol{V} \times \boldsymbol{B}) + \eta \nabla^2 \boldsymbol{B} \tag{2.6}$$

and

$$\boldsymbol{\nabla} \cdot \boldsymbol{B} = 0, \tag{2.7}$$

where $\eta = 1/\mu_0 \sigma_0$ is the Ohmic diffusion coefficient and σ_0 is the electrical conductivity.

In dense stars, plasma confinement occurs due to the strong gravitational force balanced by the electron degeneracy pressure. There exists a pressure equilibrium between these forces that confines the plasma constituents inside these stars. Thus, we include the Poisson equation of gravitational potential as

$$\nabla^2 \phi_g = 4\pi G \rho. \tag{2.8}$$

In anisotropic plasmas, the isotropic pressure is expressed by the pressure tensor

$$\overleftrightarrow{\boldsymbol{P}} = p_\perp \overleftrightarrow{\boldsymbol{I}} + (p_\parallel - p_\perp) \hat{\boldsymbol{e}} \hat{\boldsymbol{e}}, \tag{2.9}$$

where $\overleftrightarrow{\boldsymbol{I}}$ is unit dyadic and $\hat{\boldsymbol{e}} = \boldsymbol{B}/B$ is the normal vector along the direction of the magnetic field.

The CGL fluid theory applies to plasmas where collisions between particles can be neglected. These plasmas exhibit slow changes over time compared with the ion gyrating motion around a magnetic field and have spatial variations occurring over distances much greater than the ion gyration radius. The pressure components

https://doi.org/10.1017/S0022377825100445 Published online by Cambridge University Press

$p_\perp$ and $p_\parallel$ represent the adiabatic equations of state known as double-adiabatic or CGL equations which are given by

$$\frac{\mathrm{d}}{\mathrm{d}t}\left(\frac{p_\perp}{\rho B}\right)=0 \qquad \text{and} \qquad \frac{\mathrm{d}}{\mathrm{d}t}\left(\frac{p_\parallel B^2}{\rho^3}\right)=0. \tag{2.10}$$

The viscous dissipation in dense stars is an important mechanism. Binary white dwarfs come closer due to the loss of angular momentum by gravitational wave radiation and are heated internally to high temperatures due to viscous dissipation. The values of dynamical viscosity in dense stars have a wide range $\mu = 10^{11}-10^{14}$ g cm^{-1} s^{-1} (Iben *et al*. 1998). Also, the estimated viscosity parameter in the degenerate matter of density range 10^4-10^{10} g cm^{-3} lies in the range 10^2-10^{10} g cm^{-1} s^{-1} (Durisen 1973). This high viscosity value suggests the possible role of turbulence (Zahn 1977), shear and magnetic viscosity, indicating that a weak magnetic field can enhance the viscosity (Sutantyo 1974). Therefore, one cannot ignore the contribution of the viscosity of dense stars in gravitational collapse.

Thus, considering the above assumption and neglecting higher-order viscosity coefficients ($\eta_0 \gg \eta_1, \eta_2, \eta_3, \eta_4$), the Braginskii viscous stress tensor can be written as (Braginskii 1965)

$$\Pi_{xx}=\Pi_{yy}=-\frac{\eta_0}{3}\left(\frac{\partial v_x}{\partial x}+\frac{\partial v_y}{\partial y}-2\frac{\partial v_z}{\partial z}\right) \tag{2.11}$$

and

$$\Pi_{zz}=2\frac{\eta_0}{3}\left(\frac{\partial v_x}{\partial x}+\frac{\partial v_y}{\partial y}-2\frac{\partial v_z}{\partial z}\right). \tag{2.12}$$

Equations (2.3)–(2.8) represent the governing fluid equations for the considered configuration. In the model equations, the fluid pressure is considered classical to maintain the validity of the CGL fluid model. In the fluid theory, at the MHD scale, the collective wave modes and instabilities are described through the bulk plasma parameters such as classical pressure, fluid density and global fluid velocity. Thus, in most quantum plasma work, the fluid pressure is taken to be classical (Haas 2005; Shukla & Stenflo 2008; Lundin *et al*. 2008; Asenjo 2012), specifically in the present work, to adopt the CGL fluid equations in their usual form. The wave modes and instabilities in the degenerate quantum plasma can be studied with the help of analytical solutions of these equations. These equations are linearised and solved in the following section using normal-mode analysis to obtain the characteristic dispersion relations.

3. Perturbation equations and dispersion relation

Equations (2.3)–(2.8) are linearised, assuming that each quantity consists of equilibrium and perturbed parts. The equilibrium part of the physical quantity is independent of space–time variations. These physical quantities can be represented as $\rho=\rho_0+\rho_1$, $\phi_g=\phi_{0g}+\phi_{1g}$, $p_{\parallel,\perp}=p_{0\parallel,0\perp}+p_{1\parallel,1\perp}$, $\boldsymbol{V}=\boldsymbol{v}_0(=0)+\boldsymbol{v}_1$, $\boldsymbol{M}=\boldsymbol{M}_0+\boldsymbol{M}_1$, $\overleftrightarrow{\boldsymbol{P}}=\overleftrightarrow{\boldsymbol{P}}_0+\overleftrightarrow{\boldsymbol{P}}_1$, $\overleftrightarrow{\boldsymbol{\Pi}}=\overleftrightarrow{\boldsymbol{\Pi}}_0+\overleftrightarrow{\boldsymbol{\Pi}}_1$ and $\boldsymbol{B}=\boldsymbol{B}_0+\boldsymbol{B}_1$. All the quantities with subscript '0' represent the unperturbed states of physical quantities, such as the fluid velocity, pressure, density, spin-induced magnetisation, gravitational potential, viscosity tensor and magnetic field. The perturbations in these physical quantities can be expressed as ρ_1, ϕ_{1g}, $p_{1\parallel,1\perp}$, $\boldsymbol{v}_1(v_x, v_y, v_z)$, $\boldsymbol{M}_1$, $\boldsymbol{P}_1$, $\overleftrightarrow{\boldsymbol{\Pi}}_1$ and $\boldsymbol{B}_1(B_{1x}, B_{1y}, B_{1z})$,

https://doi.org/10.1017/S0022377825100445 Published online by Cambridge University Press

respectively. The magnitude of the perturbations is assumed to be small as compared with the magnitude of the unperturbed state, i.e. $|A_1| \ll |A_0|$.

Let us now write the perturbed form of the equation of motion (2.3) as

$$\rho\frac{\partial \boldsymbol{v}_1}{\partial t} = -\boldsymbol{\nabla}\cdot\overleftrightarrow{\boldsymbol{P}}_1 - \boldsymbol{\nabla}\cdot\overleftrightarrow{\boldsymbol{\Pi}}_1 - \rho\boldsymbol{\nabla}\phi_{1g} + 2\rho(\boldsymbol{v}_1\times\boldsymbol{\Omega}) - \boldsymbol{\nabla}\left(\frac{B_0B_{1z}}{\mu_0} - M_0B_{1z} - M_{1z}B_0\right) + \boldsymbol{B}_0\boldsymbol{\nabla}\left(\frac{\boldsymbol{B}_1}{\mu_0} - M_1\right) + \frac{\hbar^2}{4m_em_i}\boldsymbol{\nabla}\nabla^2\rho_1. \tag{3.1}$$

The perturbed form of the continuity equation (2.4) is

$$\frac{\partial\rho_1}{\partial t} + \rho\,(\boldsymbol{\nabla}\cdot\boldsymbol{v}_1) = 0. \tag{3.2}$$

The perturbed form of the magnetisation equation is

$$\boldsymbol{M}_1 = M_0\left(\frac{\boldsymbol{B}_{1\perp}}{B_0} + \frac{\rho_1}{\rho}\hat{\boldsymbol{z}}\right), \tag{3.3}$$

where $\boldsymbol{B}_{1\perp} = (B_{1x}, B_{1y}, 0)$ and $M_0 = (B_0/\mu_0)\chi/(1+\chi)$. Here χ is the magnetic susceptibility given by (Lundin *et al*. 2008)

$$\chi = \frac{\left((B_0\mu_B)/\left(m_iV_A^2\right)\right)\tanh\left((\mu_BB)/(k_BT)\right)}{1 - \left((B_0\mu_B)/\left(m_iV_A^2\right)\right)\tanh\left((\mu_BB)/(k_BT)\right)}. \tag{3.4}$$

The perturbed form of magnetic induction equation (2.6) and the Gauss law of magnetism (2.7) are

$$\frac{\partial\boldsymbol{B}_1}{\partial t} = \boldsymbol{\nabla}\times(\boldsymbol{v}_1\times\boldsymbol{B}_0) + \eta\nabla^2\boldsymbol{B}_1 \tag{3.5}$$

and

$$\boldsymbol{\nabla}\cdot\boldsymbol{B}_1 = 0. \tag{3.6}$$

The perturbed form of the Poisson equation of self-gravitational potential (2.8) can be written as

$$\nabla^2\phi_{1g} = 4\pi G\rho_1. \tag{3.7}$$

The perturbed form of the pressure tensor equation (2.9) is

$$\overleftrightarrow{\boldsymbol{P}}_1 = p_{1\perp}\overleftrightarrow{\boldsymbol{I}} + (p_{1\parallel} - p_{1\perp})\hat{\boldsymbol{e}}\hat{\boldsymbol{e}} + (p_\parallel - p_\perp)(\hat{\boldsymbol{e}}\hat{\boldsymbol{e}}_1 + \hat{\boldsymbol{e}}_1\hat{\boldsymbol{e}}). \tag{3.8}$$

The perturbed form of the adiabatic equations of state (2.10) is

$$\frac{p_{1\perp}}{p_\perp} = \frac{\rho_1}{\rho} + \frac{B_1}{B} \qquad \text{and} \qquad \frac{p_{1\parallel}}{p_{1\parallel}} = \frac{3\rho_1}{\rho} - \frac{2B_1}{B}. \tag{3.9}$$

These perturbation equations are solved using normal-mode analysis to derive the dispersion relations and analyse waves and instabilities in various cases. We assume small perturbations in each perturbed quantity of the form of a sinusoidal function of space and time as

$$A_1(\boldsymbol{r}, t) = A_1'\exp(i\boldsymbol{k}\cdot\boldsymbol{r} - i\omega t), \tag{3.10}$$

https://doi.org/10.1017/S0022377825100445 Published online by Cambridge University Press

where A_1' shows the amplitude of the perturbation and ω is the perturbation frequency. The wavevector $\boldsymbol{k}$ is restricted to the $x-z$ plane such that $\boldsymbol{k} = k_x\hat{\boldsymbol{x}} + k_z\hat{\boldsymbol{z}}$, where k_x and k_z represent the wavenumbers along the x and z axes, respectively. The above perturbations give rise to space and time derivatives as $\partial/\partial x = ik_x$, $\partial/\partial z = ik_z$, $\partial/\partial t = -i\omega$, respectively.

The $\hat{\boldsymbol{x}}$, $\hat{\boldsymbol{y}}$ and $\hat{\boldsymbol{z}}$ components of divergence of viscosity stress tensor $\overleftrightarrow{\boldsymbol{\Pi}}_1$ are given by

$$(\boldsymbol{\nabla}\cdot\overleftrightarrow{\boldsymbol{\Pi}}_1)_x = \frac{\eta_0}{3}\left(k_x^2 v_x - 2k_x k_z v_z\right), \tag{3.11a}$$

$$(\boldsymbol{\nabla}\cdot\overleftrightarrow{\boldsymbol{\Pi}}_1)_y = 0, \tag{3.11b}$$

$$(\boldsymbol{\nabla}\cdot\overleftrightarrow{\boldsymbol{\Pi}}_1)_z = -\frac{2\eta_0}{3}\left(k_x k_z v_x - 2k_z^2 v_z\right). \tag{3.11c}$$

The $\hat{\boldsymbol{x}}$, $\hat{\boldsymbol{y}}$ and $\hat{\boldsymbol{z}}$ components of divergence of pressure tensor as stated in (3.8) can be written as

$$(\boldsymbol{\nabla}\cdot\overleftrightarrow{\boldsymbol{p}}_1)_x = \frac{i}{\omega}\left(k_x^2 v_x + k_x k_z v_z\right)p_\perp + \frac{v_x}{\omega_\eta}\left[k_x^2 p_\perp - (p_\parallel - p_\perp)k_z^2\right], \tag{3.12a}$$

$$(\boldsymbol{\nabla}\cdot\overleftrightarrow{\boldsymbol{P}}_1)_y = -k_z^2 v_y \frac{(p_\parallel - p_\perp)}{\omega_\eta}, \tag{3.12b}$$

$$(\boldsymbol{\nabla}\cdot\overleftrightarrow{\boldsymbol{p}}_1)_z = \frac{3i}{\omega}\left(k_x k_z v_x + k_z^2 v_z\right)p_\parallel - \frac{v_x}{\omega_\eta}\left[2k_x k_z p_\parallel + (p_\parallel - p_\perp)k_x k_z\right]. \tag{3.12c}$$

Equation (3.1) is solved with the help of (3.2), (3.3), (3.5), (3.7), (3.11) and (3.12). Then after resolving the equation of motion, i.e. (3.1), in $\hat{\boldsymbol{x}}$, $\hat{\boldsymbol{y}}$ and $\hat{\boldsymbol{z}}$ components which gives three equations in terms of v_x, v_y and v_z. These equations are written in matrix form as

$$[Q]_{mn} \times [P]_q = 0, \tag{3.13}$$

where $m, n, q = 1, 2, 3$. Matrix $[P]_q$ is a column matrix of order 3×1, whose elements are v_x, v_y and v_z. Matrix $[Q]_{mn}$ is a 3×3 square matrix with the following matrix elements:

$$Q_{11} = \omega^2 - \frac{i\omega}{\omega_\eta}\left[\left(C_{s\parallel}^2 - C_{s\perp}^2 - \frac{V_A^2}{1+\chi}\right)k_z^2 - \left(C_{s\perp}^2 + \frac{V_A^2}{1+\chi}\right)k_x^2\right] - k_x^2\left(\Lambda^2 - \frac{\chi V_A^2}{1+\chi}\right) + \frac{i\omega\eta_0}{3\rho}k_x^2, \tag{3.14a}$$

$$Q_{12} = -2i\omega\Omega, \tag{3.14b}$$

$$Q_{13} = -k_x k_z\left(\Lambda^2 - \frac{\chi V_A^2}{1+\chi} + \frac{2i\omega\eta_0}{3\rho}\right), \tag{3.14c}$$

$$Q_{21} = 2i\Omega \tag{3.14d}$$

https://doi.org/10.1017/S0022377825100445 Published online by Cambridge University Press

$$Q_{22} = \omega - \frac{ik_z^2}{\omega_\eta}\left(C_{s\parallel}^2 - C_{s\perp}^2 - \frac{V_A^2}{1+\chi}\right), \tag{3.14e}$$

$$Q_{23} = 0, \tag{3.14f}$$

$$Q_{31} = -k_x k_z\left[\frac{i\omega}{\omega_\eta}\left(3C_{s\parallel}^2 - C_{s\perp}^2 + \frac{\chi V_A^2}{1+\chi}\right) - \frac{i\omega\eta_0}{3\rho} + T^2\right] \tag{3.14g}$$

$$Q_{32} = 0, \tag{3.14h}$$

$$Q_{33} = \omega^2 + \frac{i\omega 4\eta_0}{3\rho}k_z^2 - k_z^2 T^2, \tag{3.14i}$$

where $C_{s\parallel} = (p_\parallel/\rho)^{1/2}$, $C_{s\perp} = (p_\perp/\rho)^{1/2}$ and $\omega_\eta = -i\omega + \eta k^2$. The term $V_A = B/(\mu_0\rho)^{1/2}$ represents the Alfvén speed. The term $\mathcal{F}_h^2 = [C_{s\parallel}^2 - C_{s\perp}^2 - V_A^2/(1+\chi)]$ represents the pressure-anisotropy-driven firehose mode. Also, the following substitutions are used:

$$\Lambda^2 = \left(\frac{\hbar^2 k^2}{4m_e m_i} + C_{s\perp}^2 - \frac{4\pi G\rho}{k^2}\right) \quad \text{and} \quad T^2 = \left(\frac{\hbar^2 k^2}{4m_e m_i} + 3C_{s\parallel}^2 - \frac{4\pi G\rho}{k^2}\right). \tag{3.15}$$

The general dispersion relation is obtained by putting the determinant of the matrix $\det.(Q)_{mn} = 0$, given as

$$\begin{aligned}
&\left[\omega^2 - \frac{i\omega}{\omega_\eta}\left\{\mathcal{F}_h^2 k_z^2 - \left(C_{s\perp}^2 + V_A^2\frac{1}{1+\chi}\right)k_x^2\right\} + i\omega\frac{\eta_0}{3\rho}k_x^2 - \left(\Lambda^2 - \frac{\chi V_A^2}{1+\chi}\right)k_x^2\right] \\
&\quad\times\left\{\left(\omega - \frac{i}{\omega_\eta}\mathcal{F}_h^2 k_z^2\right)\left(\omega^2 + i\omega\frac{4\eta_0}{3\rho}k_z^2 - T^2 k_z^2\right)\right\} \\
&\quad - 4\Omega^2\omega\left(\omega^2 + i\omega\frac{4\eta_0}{3\rho}k_z^2 - T^2 k_z^2\right) + \left\{k_x^2 k_z^2\left(\Lambda^2 - \frac{\chi V_A^2}{1+\chi} + \frac{2i\omega\eta_0}{3\rho}\right)\right\} \\
&\quad\times\left[\left(\omega - \frac{ik_z^2}{\omega_\eta}\mathcal{F}_h^2\right)\left\{-\frac{i\omega}{\omega_\eta}\left(3C_{s\parallel}^2 - C_{s\perp}^2 + \frac{\chi V_A^2}{1+\chi}\right) + \frac{i\omega\eta_0}{3\rho} - T^2\right\}\right] = 0.
\end{aligned} \tag{3.16}$$

Equation (3.16) represents the general dispersion relation of a self-gravitating anisotropic quantum plasma consisting of viscosity tensor, spin-induced magnetisation and finite electrical resistivity in CGL limits. The shear Alfvén mode is modified to firehose mode due to pressure anisotropy in the system. The firehose mode ($\mathcal{F}_h^2$) is modified due to the spin magnetisation effects χ. In the limit of weak magnetisation ($\chi \to 0$), it gives the classical firehose instability $C_{s\parallel}^2 > C_{s\perp}^2 + V_A^2$. As magnetic susceptibility χ increases, the Alfvén velocity-dependent term in $\mathcal{F}_h^2$ decreases. Thus, the spin magnetisation helps to make the firehose modes more unstable. The dispersion relation is different from that of Lundin *et al*. (2008) due to the consideration of pressure anisotropy, rotation, viscosity and finite electrical resistivity. The above dispersion relation in the limit $\eta = \eta_0 = \Omega = 0$ and in the isotropic limit $C_{s\parallel}^2 = C_{s\perp}^2 = C_s^2$ reduces to the dispersion relation that is derived by Lundin *et al*. (2008).

https://doi.org/10.1017/S0022377825100445 Published online by Cambridge University Press

However, there are some extra C_s terms in the above dispersion relation because we consider the plasma to be a CGL fluid. In the isotropic limit and considering the system to be non-rotating ($\Omega = 0$), our dispersion relation becomes identical to the dispersion relation that is derived by Sharma & Chhajlani (2014). In the weak magnetisation limit, ignoring viscosity effects ($\chi \to 0$, $\eta_0 = 0$), equation (3.16) reduces to the dispersion relation of Bhakta & Prajapati (2018). In the above dispersion relation, the Alfvén velocity term depends on magnetic susceptibility. Thus, the firehose instability criterion and growth rate of the instability will be significantly modified due to magnetisation effects. Since the medium is rotating as a whole, the terms containing Ω signify the presence of Coriolis force in the dispersion relation.

4. Results and discussion

The perturbed state of degenerate plasmas in the interior of dense stars excites low-frequency waves, instability and turbulence. The behaviour of quantum corrections to the properties of low-frequency CGL waves and instabilities in anisotropic plasmas exhibits different features depending upon the direction of propagation of wavevector $\boldsymbol{k}$. It will be easy to analyse the dispersion properties of distinct propagation modes to visualise the effects of various considered parameters. The general dispersion relation (3.16) is discussed in the transverse ($\boldsymbol{k} \perp \boldsymbol{B}$) and longitudinal ($\boldsymbol{k} \parallel \boldsymbol{B}$) propagation modes.

4.1. *Transverse propagation ($\boldsymbol{k} \perp \boldsymbol{B}$)*

Let us discuss the dispersion properties of the system in the transverse mode by putting $k_x = k$, $k_z = 0$ in the dispersion relation. The simplified form of the dispersion relation (3.16) can be written as

$$\omega^3 \left\{ \omega^2 + i\omega \frac{\eta_0 k^2}{3\rho} + \frac{i\omega}{\omega_\eta} k^2 \left(C_{s\perp}^2 + \frac{V_A^2}{1+\chi} \right) - 4\Omega^2 - k^2 \left(\Lambda^2 - \frac{\chi}{1+\chi} V_A^2 \right) \right\} = 0. \tag{4.1}$$

The first factor of the above equation gives $\omega = 0$, which suggests the non-propagating mode called the entropy mode. This is a universal mode in plasmas because the density gradient is the driving force of this mode (Rogers, Zhu & Francisquez 2018). Another mode which consists of the effects of various considered parameters is obtained by putting $\omega = i\sigma$:

$$\begin{aligned} &\sigma^3 + k^2 \left(\eta + \frac{\eta_0}{3\rho} \right) \sigma^2 + \left(\Lambda^2 k^2 + \bar{\chi} V_A^2 k^2 + \frac{\eta_0}{3\rho} \eta k^4 + C_{s\perp}^2 k^2 + 4\Omega^2 \right) \sigma \\ &+ \eta k^2 \left(\Lambda^2 k^2 - \frac{\chi}{1+\chi} V_A^2 k^2 + 4\Omega^2 \right) = 0, \end{aligned} \tag{4.2}$$

where $\bar{\chi} = (1-\chi)/(1+\chi)$.

This shows a damped viscous Alfvén mode modified due to magnetisation, rotation and Ohmic dissipative effects. The viscous damping and frictional dissipation play a major role in the MHD wave dissipation in the solar atmosphere. The source of viscous damping is the momentum transfer during the thermal motion of particles, and the frictional dissipation is represented by the electrical resistivity (Gordon & Hollweg 1983; Khodachenko *et al*. 2004). The Jeans instability and gravitational collapse described in the transverse mode are significantly affected by the consideration

https://doi.org/10.1017/S0022377825100445 Published online by Cambridge University Press

of magnetisation and rotation in quantum plasmas. In the quantum regime, these effects may give rise to new dissipative modes. In the absence of spin magnetisation and viscosity ($\chi = \eta = 0$), we get the dispersion relation (24) of Bhakta & Prajapati (2018). Ignoring the role of pressure anisotropy for the isotropic quantum plasma and rotation ($\Omega = 0$), this mode becomes identical to equation (22) of Sharma & Chhajlani (2014).

According to the Routh–Hurwitz criterion, the constant part decides the stability of the system. The necessary stability condition demands the constant part to be positive; otherwise, the system will be unstable. Hence, the condition of instability derived from (4.2) for the system is given by

$$k^2\left(\Lambda^2 - \frac{\chi}{1+\chi}V_A^2\right) + 4\Omega^2 < 0. \tag{4.3}$$

Therefore, the critical Jeans wavenumber is given by

$$k_{J_1}^2 = \frac{2m_e m_i}{\hbar^2}\left(C_{s\perp}^2 - \frac{\chi}{1+\chi}V_A^2\right) \times \left\{\left(1 + \frac{4\hbar^2(\pi G\rho - \Omega^2)}{m_e m_i\left(C_{s\perp}^2 - (\chi/(1+\chi))V_A^2\right)^2}\right)^{1/2} - 1\right\}. \tag{4.4}$$

The conditions (4.3) and (4.4) respectively show the modified Jeans instability criterion and expression of the critical Jeans wavenumber in anisotropic quantum plasmas. The presence of uniform rotation, quantum diffraction and magnetisation directly influences the Jeans instability criterion. For perturbation wavenumber $k < k_{J_1}$, the system will be unstable, which means that for perturbation wavelength $\lambda > \lambda_{J_1}$, the system will become gravitationally unstable. Interestingly, if the rotation exceeds a critical value $\Omega_c = \sqrt{\pi G\rho}$, the system will be entirely stable. This criterion is similar to that given by Tandon & Talwar (1963) for classical anisotropic plasmas. Thus, the threshold wavenumber that determines the Jeans instability has been modified significantly at the quantum scale. We calculate the critical rotational frequency of a white dwarf taking the mass density parameter $\rho = 3 \times 10^9$ kg m^{-3} (Shukla, Mendis & Krasheninnikov 2011) which is measured to be $\Omega_c \approx 0.8$ s^{-1}. We have the fastest-rotating white dwarfs with a time period of approximately $r_p = 25$ s (Pelisoli *et al*. 2021), giving a rotational frequency of about $\Omega = 0.25$ s^{-1}. The rotational velocity value of even the fastest-rotating white dwarf does not satisfy the condition of complete stability ($\Omega > \Omega_c$) due to rotation. This suggests that the Coriolis force alone does not predict the gravitational stability of white dwarfs.

Along with this, we have an additional condition which determines the instability of the considered system. If the magnetised system is such that the condition $C_{s\perp} = \sqrt{\chi/(1+\chi)}V_A$ is satisfied, then the system will be a gravitationally stable system against all the perturbation wavenumbers. The effects of the magnetic field appear in the condition of instability because of the magnetisation in the plasma, making the equation more realistic. The instability criterion is unaffected due to the viscosity and resistivity effects, which confirms the results of previous works (Sharma & Chhajlani 2014; Sangwan & Prajapati 2023). The analytical results can be applied to understand the Jeans instability in quantum plasmas of magnetised dense white dwarfs. To measure the Jeans wavelength and Jeans mass, we take the plasma parameters in the interior of the white dwarf as shown in table 1. The calculated values of critical Jeans wavenumber $k_{J_1} \simeq 3.76 \times 10^{-7}$ m^{-1} and corresponding Jeans wavelength $\lambda_{J_1} \simeq 1.8 \times 10^3$ km suggest that white dwarfs must have

https://doi.org/10.1017/S0022377825100445 Published online by Cambridge University Press

Physical quantity	Symbol	Value	Units
Gravitational constant	G	6.67×10^{-11}	$\mathrm{N\,m^2\,kg^{-2}}$
Ion mass	m_i	$4 \times 6.67 \times 10^{-27}$	kg
Electron mass	m_e	9.1×10^{-31}	kg
Perpendicular sound speed	$C_{s\perp}$	4×10^6	$\mathrm{m\,s^{-1}}$
Magnetic field	B	10^5	T
Alfvén velocity	V_A	1.6×10^3	$\mathrm{m\,s^{-1}}$
Rotational frequency	Ω	0.25	$\mathrm{s^{-1}}$
Magnetic susceptibility	χ	3	Unitless

TABLE 1. Plasma parameters of magnetised degenerate white dwarfs (Lou 1995; Lundin *et al.* 2008; Shukla *et al.* 2011; Pelisoli *et al.* 2021).

a radius larger than this value to be gravitationally unstable. Corresponding to the above Jeans length, the estimated Jeans mass is $M_{J_1} = 0.04 M_\odot$, which is in the range of that of some known white dwarfs. The Jeans frequency for a white dwarf is $\omega_j \simeq 1.6\ \mathrm{s^{-1}}$, which shows that the time of collapse is very short.

The magnetic susceptibility χ depends upon the magnetic field, density and temperature. A gradual change in these parameters will change χ and characterise plasmas to be unmagnetised ($\chi = 0$), paramagnetic ($\chi \leqslant 1$) and ferromagnetic ($\chi \gg 1$). The Jeans instability criterion and gravitational collapse will differ in these limiting cases. For unmagnetised plasmas ($\chi, V_A = 0$), the Jeans wavenumber becomes independent of the magnetic field and dependent on $C_{s\perp}$ on V_A as defined in expression (4.4) for the system to be gravitationally unstable. In the strong magnetisation limit ($\chi \gg 1$), the gravitational instability criterion (4.4) is satisfied provided that $C_{s\perp} > V_A$, which holds well in the degenerate stellar interior (Lou 1995). From criterion (4.4), it is clear that in the strong magnetisation limit ($\chi \gg 1$), the term $\chi/(1+\chi) \to 1$, and thus the Alfvén velocity term becomes independent of χ. In this case, an increase in the magnetic field (Alfvén velocity) will also increase k_{J_1}, which will enhance the growth rate of instability. On the other hand, the effect of weak magnetisation ($\chi \ll 1$) reduces the value of the magnetic field, making k_{J_1} smaller and stabilising the growth rate of the instability. Such an effect of the magnetic field on the growth rates in both weak and strong magnetisation limits is observed later in figure 4.

The dispersion relation (4.2) is discussed in limiting cases of interest to examine the influence of various physical parameters. Let us discuss it for the case of infinitely conducting quantum plasmas, i.e. $\eta = 0$, which gives

$$\sigma^2 + \frac{\eta_0 k^2}{3\rho}\sigma + \Lambda^2 k^2 + \left(\frac{1-\chi}{1+\chi}\right) V_A^2 k^2 + C_{s\perp}^2 k^2 + 4\Omega^2 = 0. \tag{4.5}$$

The condition of instability can be written from the constant term as

$$k^2 \left\{ \Lambda^2 + \left(\frac{1-\chi}{1+\chi}\right) V_A^2 + C_{s\perp}^2 \right\} + 4\Omega^2 < 0. \tag{4.6}$$

This condition is modified due to the effects of rotation and pressure anisotropy in CGL plasmas. In an isotropic quantum plasma neglecting rotation, the

https://doi.org/10.1017/S0022377825100445 Published online by Cambridge University Press

above instability condition becomes identical to the instability condition (18) of Lundin *et al.* (2008). The modified expression of Jeans wavenumber is obtained as

$$k_{J_2}^2 = \frac{2m_e m_i}{\hbar^2}\left(2C_{s\perp}^2 + \bar{\chi} V_A^2\right)\left\{\left(1 + \frac{4\hbar^2\left(\pi G\rho - \Omega^2\right)}{m_e m_i\left(2C_{s\perp}^2 + \bar{\chi} V_A^2\right)^2}\right)^{1/2} - 1\right\}. \tag{4.7}$$

The two distinct Jeans instability criteria (4.4) and (4.7) are obtained for resistive and non-resistive plasmas, respectively. In the case of resistive quantum plasmas ($\eta \neq 0$), without magnetisation effect ($\chi = 0$), the effects of the magnetic field disappear from the instability criterion (4.4). On the other hand, in the non-resistive quantum plasma ($\eta = 0$), the effects of the magnetic field remain in the condition of Jeans instability even when $\chi = 0$. Therefore, electrical resistivity determines the role of the magnetic field in the Jeans instability criterion for the considered system.

To study the growth rate of Jeans instability, we plot the normalised growth rate versus the normalised wavenumber and vary different parameters like quantum diffraction parameter, viscosity, magnetisation, etc., and study the impact of these quantities on the growth rate of Jeans instability. The dispersion relation (4.2) is normalised by dividing it by Jeans frequency ω_j $(= \sqrt{4\pi G\rho})$ and written in dimensionless form as

$$\sigma^{*3} + k^{*2}\left(\eta^* + \frac{\eta_0^*}{3}\right)\sigma^{*2} + \left(\frac{H^{*2}k^{*4}}{4} + 2k^{*2} - 1 + \bar{\chi} V_A^{*2}k^{*2} + \frac{1}{3}\eta_0^*\eta^* k^{*4} + 4\Omega^{*2}\right)\sigma^*$$
$$+ \eta^* k^{*2}\left(\frac{H^{*2}k^{*4}}{4} - \frac{\chi}{1+\chi}V_A^{*2}k^{*2} + k^{*2} - 1 + 4\Omega^{*2}\right) = 0. \tag{4.8}$$

The dimensionless parameters used here are given as

$$\sigma^* = \frac{\sigma}{\omega_j}, \quad k^* = \frac{kC_{s\perp}}{\omega_j}, \quad H^* = \frac{\hbar\omega_j}{\sqrt{m_i m_e}C_{s\perp}^2}, \quad \eta^* = \frac{\eta\omega_j}{C_{s\perp}^2},$$
$$\eta_0^* = \frac{\eta_0\omega_j}{\rho C_{s\perp}^2}, \quad \Omega^* = \frac{\Omega}{\omega_j} \quad \text{and} \quad V_A^* = \frac{V_A}{C_{s\perp}}. \tag{4.9}$$

In figure 1, the effects of quantum correction and viscosity coefficient are illustrated on the growth rate of the Jeans instability versus wavenumber. Equation (4.8) gives three distinct roots, out of which real roots of σ^* give the unstable modes in a gravitating plasma called the growth rate of the Jeans instability. To calculate the roots, the constant values of the parameters are chosen to be $\eta^* = 4.0$, $\Omega^* = 0.5$, $V_A^* = 2.1$ and $\chi = 3$. From the subplots, it is obvious that the growth rate of Jeans instability is decreased due to an increase in the viscosity parameter for all values of the quantum correction parameter (H^*). Further, the quantum correction parameter stabilises the unstable region by suppressing the growth rate of the instability. The instability region is reduced due to increased values of H^*. For the considered wavenumber regime, the peak values of the growth rates also decrease due to an increase in the viscosity and quantum diffraction parameters. Thus, viscous dissipation and quantum effects significantly affect the gravitational collapse rate of dense stars. The quantum effects are most significant corresponding

https://doi.org/10.1017/S0022377825100445 Published online by Cambridge University Press

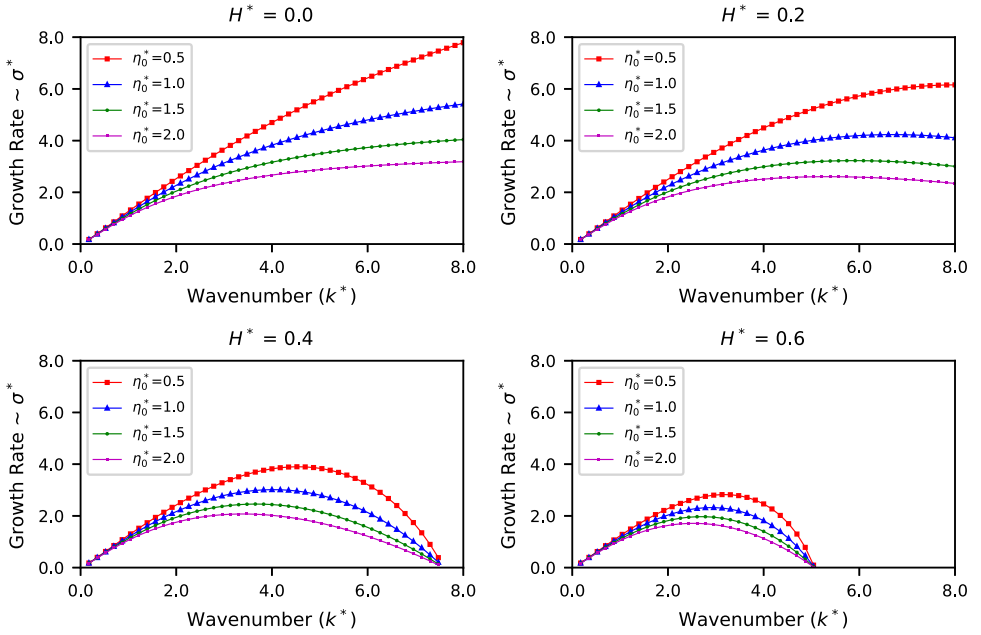

FIGURE 1. The various subplots show the combined effects of viscosity and quantum diffraction parameters on the growth rate of Jeans instability (Re σ^*) versus the normalised wavenumber (k^*) in transverse mode. The constant values of other parameters are taken to be $\eta^* = 4.0$, $\Omega^* = 0.5$, $V_A^* = 2.1$ and $\chi = 3$.

to the higher values of perturbation wavenumbers or the lower values of perturbation wavelengths. As the quantum diffraction parameter increases, the instability gets suppressed when we move towards larger values of k^*.

In figure 2, the effects of uniform rotation along with electrical resistivity are shown on the growth rate of the Jeans instability. The growth rate is plotted with the normalised wavenumber by varying the rotation and resistivity parameters and keeping other normalised parameters $\eta_0^* = 2.0$, $V_A^* = 1.8$, $H^* = 0.5$ and $\chi = 20$ to be fixed. The curves with $\eta^* = 0$ illustrate the growth rate for the non-resistive quantum plasmas. In this case, the growth rate falls rapidly with an increase in the wavenumber, which means that in such a case the system is more stable towards Jeans instability. The pulsation period of a star is a measure of its rotation. The fastest-rotating neutron star has a period of $r_p = 5$ ms. The rotation provides the centrifugal force, which assists the internal pressure against the gravitational pressure. The same effect is noticeable from the curve, which shows that rotation in the system suppresses the growth rate of Jeans instability for both non-resistive and resistive plasmas. The suppression in the growth rate due to rotation is notably fast in the shorter-wavenumber regime. As we move towards large values of wavenumbers, the suppression in the growth rate becomes weak.

White dwarfs have a wide range of rotational periods from years to a few minutes, the rotational velocity tending to increase with increased magnetic field strength (Ferrario & Wickramasinghe 2005). The merger of two white dwarfs can enormously increase the rotational velocity. EUVE J0317-853, a result of merging two white dwarfs, is an example of a highly rotating white dwarf (Ferrario *et al*. 1997).

https://doi.org/10.1017/S0022377825100445 Published online by Cambridge University Press

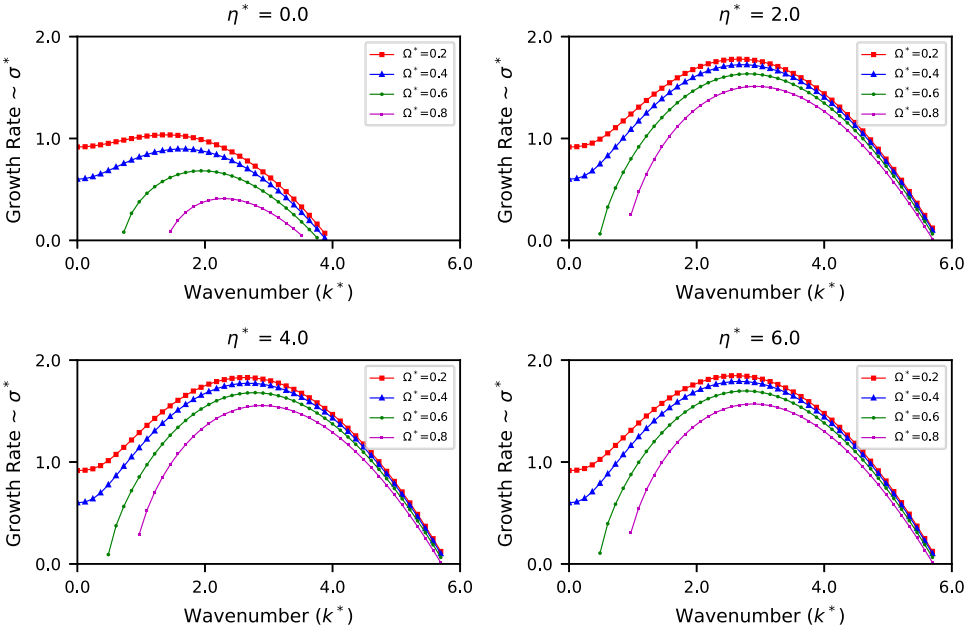

FIGURE 2. The various subplots show the combined effects of rotation and resistivity for strong magnetisation ($\chi = 20$) on the growth rate of Jeans instability ($Re\ \sigma^*$) versus the normalised wavenumber (k^*) in transverse mode. The constant values of other parameters are taken to be $\eta_0^* = 2.0$, $V_A^* = 1.8$ and $H^* = 0.5$.

The rotational effect provides extra stability to this white dwarf against gravitational collapse. The increase in the resistivity parameter has an almost negligible change in the growth rate of instability. The growth shows a similar pattern of instability region for all the resistivity parameter values except for $\eta^* = 0.0$. Thus, highly rotating and non-resistive quantum plasmas lead to a more stable state against gravitational collapse.

The magnetisation in quantum plasmas is associated with the enhanced influence of magnetic fields on the behaviour of charged particles, incorporating quantum effects such as Landau quantisation. It is challenging to achieve and maintain a strong magnetic field experimentally. However, the present theoretical analysis can be used to discuss the Jeans instability and gravitational collapse in strongly magnetised white dwarfs. Graphically, the effects of magnetisation in non-resistive and resistive quantum plasmas on the growth rate of Jeans instability are illustrated in figure 3. The normalised growth rate is plotted for magnetic susceptibility parameter $\chi = 0.5,\ 3.5,\ 6.5$ and 9.5 taking electrical resistivity parameter $\eta^* = 0.0,\ 2.0,\ 4.0$ and 6.0. In the case of a non-resistive quantum plasma with a weak magnetisation effect ($\eta^* = 0.0,\ \chi \to 0$), the growth rate is completely suppressed, and the instability region has disappeared. The weakly magnetised system is found to be more stable towards Jeans instability. The magnetisation effect significantly enhances the growth rate of the instability in both resistive and non-resistive quantum plasmas. The strong magnetisation in a quantum plasma plays a crucial role in modifying wave propagation characteristics and Jeans instability. In figure 3, it is found that the resistivity parameter has an almost negligible change in the

https://doi.org/10.1017/S0022377825100445 Published online by Cambridge University Press

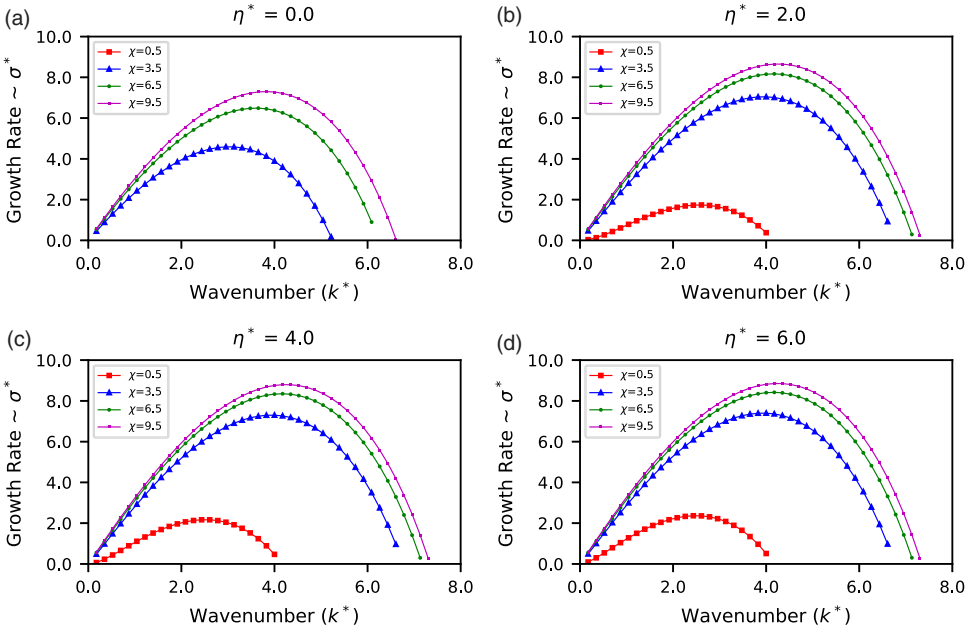

FIGURE 3. The various subplots show the combined effects of magnetisation and resistivity on the growth rate of Jeans instability (Re σ^*) versus the normalised wavenumber (k^*) in transverse mode. The constant values of other parameters are taken to be $\eta_0^* = 1.5$, $\Omega^* = 0.5$, $V_A^* = 4.0$, $H^* = 1.0$.

growth rate. In non-resistive quantum plasmas $\eta^* = 0.0$ (figure 3*a*), the instability region is clearly distinguishable from the resistive case $\eta^* \neq 0$ (figure 3(*b–d*)). However, if we compare the growth rates among the subplots, figure 3(*b–d*), of resistive plasmas, we find that there is almost negligible change in the growth rates of instability.

The effects of the magnetic fields in terms of Alfvén velocity on the growth rate of Jeans instability in both weak and strong magnetisation limits are illustrated. The results are very interesting as we get both a stabilising and destabilising influence of magnetic fields on the growth rate of instability. Figure 4 is plotted for the growth rate of Jeans instability in the case of non-resistive quantum plasma ($\eta^* = 0.0$) and keeping various other normalised parameters as $\eta_0^* = 0.2$, $\Omega^* = 0.02$, $H^* = 0.01$. In the weak magnetisation limit ($\chi = 0.5$), the growth rate decreases as the Alfvén velocity increases. However, in the strong magnetisation limit ($\chi = 3.0$), we get the reverse effect of the Alfvén velocity on the growth rate, observing its destabilising effect. Since magnetisation itself has a destabilising effect (figure 3), the increase in the magnetic field (i.e. Alfvén velocity) aligns all spins in the same direction which enhances the growth rate of the Jeans instability. It is also evident from the dispersion relation (4.8) that the appearance of parameter $\bar{\chi}$ gives rise to both stabilising and destabilising influence of the Alfvén velocity. In the weak magnetisation limit, $\bar{\chi}$ remains positive. Thus, it shows the stabilising behaviour similar to rotation, quantum diffraction and viscosity parameters. But, in the strong magnetisation limit ($\chi > 1$), $\bar{\chi}$ becomes negative, which turns the damped Alfvén mode into the growing modes supporting the growth of the Jeans instability.

https://doi.org/10.1017/S0022377825100445 Published online by Cambridge University Press

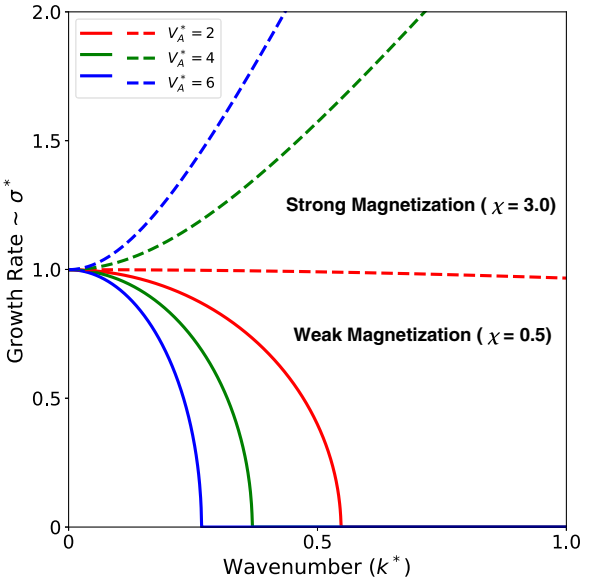

FIGURE 4. Effects of magnetic field on the growth rate of Jeans instability in weak ($\chi < 1$) and strong ($\chi > 1$) magnetisation limits keeping $\eta^* = 0.0$, $\eta_0^* = 0.2$, $\Omega^* = 0.02$ and $H^* = 0.01$ to be fixed.

4.2. *Longitudinal propagation ($\boldsymbol{k} \parallel \boldsymbol{B}$)*

In the transverse mode, the firehose instability is not observed in the dispersion relation of Jeans instability. To discuss the firehose instability and the role of pressure anisotropy, the general dispersion relation (3.16) must be discussed in different orientations. Let us simplify the dispersion relation (3.16) for the longitudinal propagation mode by putting $k_z = k$ and $k_x = 0$. In this way, we get

$$\omega\left(\omega^2 - k^2T^2 + \frac{4i\eta_0\omega}{3\rho}k^2\right)\left\{\left(\omega - \frac{ik^2}{\omega_\eta}\mathcal{F}_h^2\right)^2 - 4\Omega^2\right\} = 0. \tag{4.10}$$

The dispersion relation gives a non-propagating entropy mode corresponding to $\omega = 0$. The first factor of (4.10) can be simplified and written by putting $\omega = i\sigma$ as

$$\sigma^2 + \frac{4\eta_0}{3\rho}k^2\sigma + k^2\left(\frac{\hbar^2k^2}{4m_em_i} + 3C_{s\parallel}^2 - \frac{4\pi G\rho}{k^2}\right) = 0. \tag{4.11}$$

This dispersion relation shows the influence of viscosity and quantum corrections on the Jeans instability in the longitudinal mode. No effects of spin magnetisation and Ohmic diffusivity were observed as seen in the transverse mode (see (4.1)). Thus, the dispersion characteristics and Jeans instability criterion will differ in the longitudinal and transverse modes. A comparison of the growth rates will show the influence of various parameters in these modes. The Jeans instability criterion can be derived using the Routh–Hurwitz method and given by

$$k_{J_3}^2 = \frac{6C_{s\parallel}^2m_em_i}{\hbar^2}\left\{\left(1 + \frac{4\pi\hbar^2G\rho}{9C_{s\parallel}^4m_em_i}\right)^{1/2} - 1\right\}. \tag{4.12}$$

https://doi.org/10.1017/S0022377825100445 Published online by Cambridge University Press

The system will be gravitationally unstable in the longitudinal mode for all perturbation wavenumbers $k < k_{J_3}$. This instability criterion (4.12) is identical to the condition as derived by Sangwan & Prajapati (2023) putting polytropic index $\beta = 3$ (for CGL plasmas) in that case. The expression shows that the quantum term affects the instability criteria, whereas it is unaffected due to the magnetisation in the plasmas.

The growth rate of Jeans instability, which is mainly responsible for the structure formation in the universe, is calculated in the longitudinal mode of propagation by normalising (4.11). The normalised equation is given as

$$\sigma^{*2} + \frac{4\hat{\eta}_0\hat{k}^2}{3}\sigma^* + \left(\frac{\hat{H}^2\hat{k}^4}{4} + 3\hat{k}^2 - 1\right) = 0. \tag{4.13}$$

The various quantities are defined as

$$\sigma^* = \frac{\sigma}{\omega_j}, \quad \hat{k} = \frac{kC_{s\parallel}}{\omega_j}, \quad \hat{H} = \frac{\hbar\omega_j}{\sqrt{m_i m_e}C_{s\parallel}^2}, \quad \hat{\eta}_0 = \frac{\eta_0\omega_j}{\rho C_{s\parallel}^2}. \tag{4.14}$$

The second factor of (4.10) can be simplified and written as

$$\begin{aligned}
&\sigma^4 + 2\eta k^2\sigma^3 + \left\{\eta^2k^4 + 4\Omega^2 - 2k^2\left(C_{s\parallel}^2 - C_{s\perp}^2 - \frac{V_A^2}{1+\chi}\right)\right\}\sigma^2 \\
&+ 2\eta k^2\left\{4\Omega^2 - k^2\left(C_{s\parallel}^2 - C_{s\perp}^2 - \frac{V_A^2}{1+\chi}\right)\right\}\sigma \\
&+ k^4\left\{4\Omega^2\eta^2 + \left(C_{s\parallel}^2 - C_{s\perp}^2 - \frac{V_A^2}{1+\chi}\right)^2\right\} = 0.
\end{aligned} \tag{4.15}$$

The above dispersion relation represents a fourth-order polynomial, including the effects of rotation, spin magnetisation, Ohmic diffusivity and pressure anisotropy, independent of self-gravitation and viscosity. Once the pressure anisotropy becomes sufficiently large, the firehose instability is triggered. In the absence of rotation ($\Omega = 0$) and resistivity ($\eta = 0$), we get the fundamental firehose instability criterion ($p_\parallel > p_\perp + B^2/2\mu_0$). The pressure anisotropy turns the pure Alfvén mode into the unstable firehose mode. In the absence of magnetisation ($\chi = 0$), the dispersion relation (4.15) becomes identical to the dispersion relation (18) of Bhakta & Prajapati (2018) neglecting effects of Hall current in that case.

The condition of firehose instability from (4.15) is written as

$$C_{s\parallel}^2 > C_{s\perp}^2 + \frac{V_A^2}{1+\chi}. \tag{4.16}$$

The fundamental firehose instability criterion is modified due to the effect of spin magnetisation. If this condition is satisfied, the system will be dynamically unstable and show the firehose instability. The parameters resistivity, rotation and quantum diffraction do not affect the firehose criteria, whereas spin magnetisation supports the firehose instability. Thus, a strongly magnetised system is dynamically more unstable towards the firehose instability.

To study the growth rate, we normalised the dispersion relation (4.15), dividing it by $C_{s\perp}^4k^4$ throughout. The growth rate is studied with respect to normalised Alfvén

https://doi.org/10.1017/S0022377825100445 Published online by Cambridge University Press

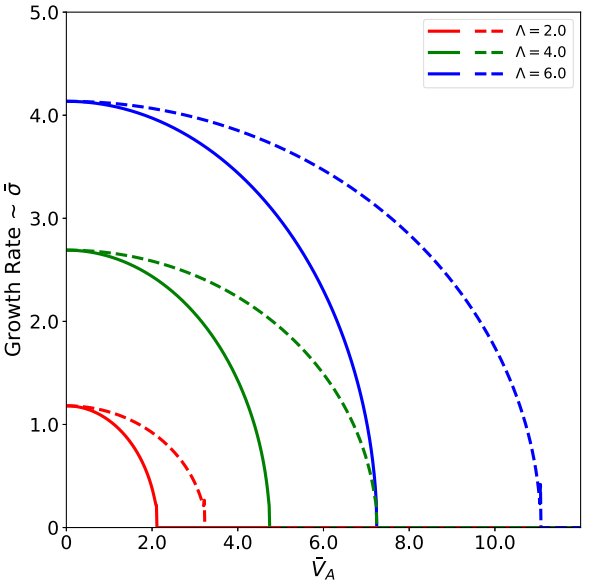

FIGURE 5. Influence of pressure anisotropy (Λ) on the growth rate of firehose instability in weak ($\chi = 0.5$, solid lines) and strong ($\chi = 2.5$, dashed lines) magnetisation limits keeping $\bar{\eta} = 0.1$ and $\bar{\Omega} = 0.1$ fixed.

velocity by varying the anisotropy in the system. The normalised dispersion relation is given as

$$\bar{\sigma}^4 + 2\bar{\eta}\bar{\sigma}^3 + \left\{\bar{\eta}^2 + 4\bar{\Omega}^2 - 2\left(\Lambda^2 - \frac{\bar{V}_A^2}{1+\chi} - 1\right)\right\}\bar{\sigma}^2 + 2\bar{\eta}\left\{4\bar{\Omega}^2 - \left(\Lambda^2 - \frac{\bar{V}_A^2}{1+\chi} - 1\right)\right\}\bar{\sigma} + 4\bar{\eta}^2\bar{\Omega}^2 + \left(\Lambda^2 - \frac{\bar{V}_A^2}{1+\chi} - 1\right)^2 = 0. \tag{4.17}$$

The following dimensionless parameters are used here:

$$\bar{\sigma} = \frac{\sigma}{kC_{s\perp}}, \quad \bar{\eta} = \frac{\eta k}{C_{s\perp}}, \quad \bar{\Omega} = \frac{\Omega}{kC_{s\perp}}, \quad \bar{V}_A = \frac{V_A}{C_{s\perp}} \quad \text{and} \quad \Lambda = \frac{C_{s\parallel}}{C_{s\perp}}. \tag{4.18}$$

In white dwarfs, the degenerate plasma pressure is isotropic on average. In the presence of a magnetic field, the electron gas becomes anisotropic because the pressure and the behaviour of electrons depend on the direction relative to the magnetic field. The effect of the strong magnetic field in compact stars is the main reason for producing pressure anisotropy which causes the deformation of these dense stars (Terrero *et al*. 2019). In addition, the rotational effects in white dwarfs can also introduce anisotropy. The centrifugal force due to rotation causes a white dwarf to become oblate, leading to different pressure gradients in different directions. Let us study the impact of pressure anisotropy on the growth rate of firehose instability in dense magnetised quantum plasmas. In figure 5, the growth rate of firehose instability ($\bar{\sigma}$) is depicted versus the normalised Alfvén velocity ($\bar{V}_A$) for various values

https://doi.org/10.1017/S0022377825100445 Published online by Cambridge University Press

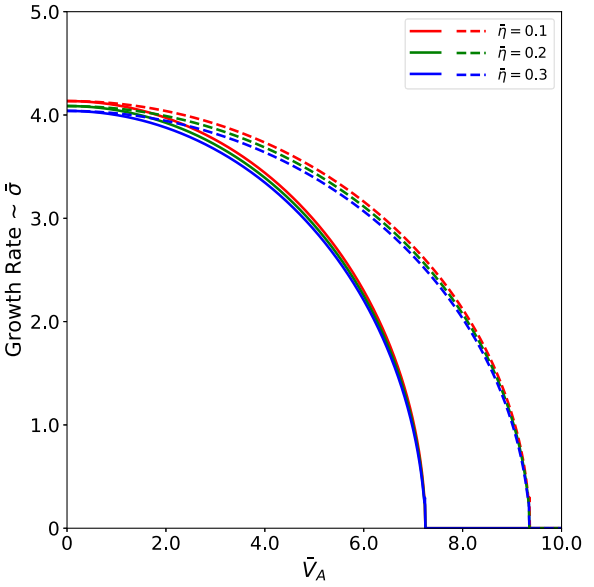

FIGURE 6. Influence of resistivity ($\bar{\eta}$) on the growth rate of firehose instability in weak ($\chi = 0.5$, solid lines) and strong ($\chi = 1.5$, dashed lines) magnetisation limits keeping $\bar{\Omega} = 0.1$ and $\Lambda = 6.0$ fixed.

of pressure anisotropy parameter $\Lambda = 2.0,\ 4.0,\ 6.0$, keeping the other normalised parameters fixed as $\bar{\eta} = 0.1,\ \bar{\Omega} = 0.1$. The curves are plotted in both the strong magnetisation limit taking $\chi = 2.5$ (dashed curves) and the weak magnetisation limit with $\chi = 0.5$ (solid lines). The curves show that as the pressure anisotropy of the system increases, the instability region becomes larger, showing that the highly anisotropic system is more favourable to the firehose instability. In the strong magnetisation case, the instability region is observed to be larger than in the weak magnetisation case. The peak value of the growth rate also increases due to increased pressure anisotropy. Thus, pressure anisotropy, together with spin magnetisation, destabilises the growth rate of firehose instability in dense quantum plasmas.

In figure 6 the normalised growth rate ($\bar{\sigma}$) versus the normalised Alfvén velocity ($\bar{V}_A$) is plotted for various values of normalised resistivity $\bar{\eta} = 0.1$, 0.2 and 0.3, keeping the normalised rotational velocity $\bar{\Omega} = 0.1$ and anisotropy $\Lambda = 6.0$ to be constant. The curve is plotted for both strongly magnetised (dashed lines) and weakly magnetised (solid lines) systems. The growth rate of firehose instability decreases with an increase in the resistivity of the system for both strongly and weakly magnetised systems. The highly magnetised systems are less stable towards the firehose instability than weakly magnetised systems. The Alfvén velocity is higher in strongly magnetised plasmas for which the firehose instability growth rate is completely suppressed.

In figure 7, the firehose growth rate versus the normalised Alfvén velocity is plotted for various values of normalised rotational velocity $\bar{\Omega} = 0.5$, 1.0 and 1.5 keeping the normalised resistivity $\bar{\eta} = 0.15$ and anisotropy $\Lambda = 6.0$ to be constant. The growth rate of firehose instability is greater for systems having larger rotational velocity and high intrinsic magnetisation. The instability growth shows a large divergence in both strongly and weakly magnetised systems, suggesting that there is a

https://doi.org/10.1017/S0022377825100445 Published online by Cambridge University Press

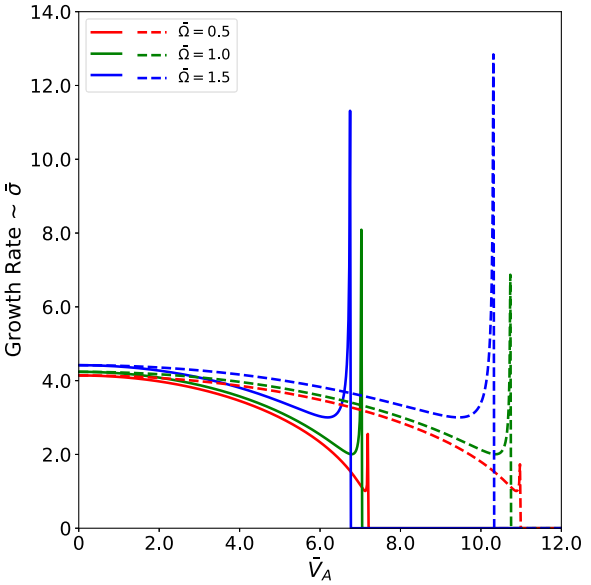

FIGURE 7. Influence of rotation ($\bar{\Omega}$) on the growth rate of firehose instability in weak ($\chi = 0.5$, solid lines) and strong ($\chi = 2.5$, dashed lines) magnetisation limits keeping $\bar{\eta} = 0.15$ and $\Lambda = 6.0$ fixed.

cutoff Alfvén velocity at which growth rates increase sharply, making the system highly firehose unstable. The firehose instability region is extended towards higher values of the Alfvén velocity in a strong magnetisation limit. There are sudden spikes in the growth rate of firehose instability at some specific values of Alfvén velocity which points out the possibility of some resonance effects between the particles and Alfvén waves in the plasmas. The firehose instability is sensitive to the velocity distribution of particles. There are some values of Alfvén velocity over which certain populations of particles interact strongly with the wave modes associated with the firehose instability, leading to a sudden increase in the growth rate of instability. These specific Alfvén velocities can vary with the rotational velocity and also with the magnetisation in the system.

In figure 8, the effects of the quantum term on the growth rate of Jeans instability are compared in transverse mode (solid lines; using (4.8)) and longitudinal mode (dotted lines; using (4.13)). The normalised growth (σ^*) rates versus the normalised wavenumber (k^* and $\hat{k}$) are plotted by keeping other parameters $\hat{\eta}_0 = \eta_0^* = 2.0$, $\eta^* = 1.0$, $V_A^* = 4$, $\Omega^* = 0.02$ and $\chi = 0.5$ to be fixed. In both modes, the growth rate is suppressed due to the quantum diffraction parameter. Since the quantum effects are important for small wavelengths, they effectively suppress the Jeans instability growth rate in both longitudinal and transverse modes for smaller wavelengths. In the longitudinal mode, the growth rate is completely suppressed, whereas in the transverse mode the instability growth rate seems to diverge for small H^*. The cutoff wavenumbers at which the growth rate becomes zero in the longitudinal mode are smaller than in the transverse mode. The region of instability is smaller for the transverse mode due to the presence of rotation, resistivity and magnetic field which reduces the instability region. In the transverse mode, the growth rate of instability is completely suppressed if the quantum term is large. Otherwise, the growth of the

https://doi.org/10.1017/S0022377825100445 Published online by Cambridge University Press

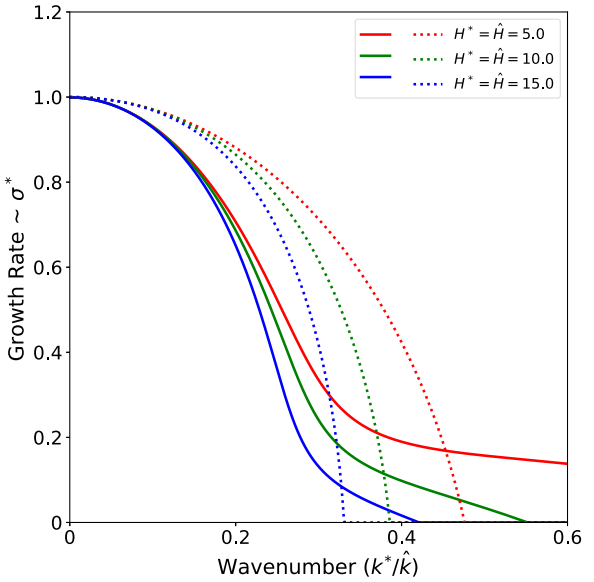

FIGURE 8. The effects of quantum parameter with comparison of growth rates of Jeans instability in longitudinal mode (dotted lines) and transverse mode (solid lines) keeping the constant values $\hat{\eta_0} = \eta_0^* = 2.0$, $\eta^* = 1.0$, $V_A^* = 4$, $\Omega^* = 0.02$ and $\chi = 0.5$.

Jeans instability seems to diverge. Thus, the nature of instability completely depends upon the orientation of wave propagation and other physical parameters.

5. Conclusions

This paper investigates the pressure-anisotropy-driven firehose and gravitational instabilities in spin-magnetised dense quantum plasmas considering the effects of Ohmic diffusion and viscosity stress tensor. The general dispersion properties of waves and instabilities have been discussed in the longitudinal and transverse propagation modes. In the transverse mode, in addition to the entropy mode, the modified dispersion relation of the Jeans instability is obtained, which results in a significant change in the Jeans instability criterion and Jeans wavenumber. In non-resistive quantum plasmas, the Jeans instability criterion depends on the magnetic field, even when spin magnetisation is neglected. The growth rate of Jeans instability in non-resistive quantum plasmas is sensitive to spin magnetisation. In a weak magnetisation limit, the magnetic field suppresses the growth rate of instability, whereas in a strong magnetisation limit, it enhances the growth rate of Jeans instability. The quantum diffraction, viscosity and rotation parameters play a crucial role in reducing the growth rate, while spin magnetisation enhances the growth rate of the Jeans instability in anisotropic quantum plasmas. In resistive quantum plasmas, there is a trivial change in the growth rates due to an increase in the Ohmic diffusion coefficient. However, it gives an additional wave mode in the dispersion relation by modifying the instability criterion. The Jeans instability region is smaller in the transverse mode than in the longitudinal mode up to the cutoff wavenumbers, beyond which it is enhanced due to additional factors present in the dispersion relation.

In the longitudinal mode, the dispersion properties of Jeans instability remain independent of spin magnetisation and Ohmic diffusion effects. The firehose mode has been modified due to rotation, spin magnetisation and electrical resistivity. The spin

https://doi.org/10.1017/S0022377825100445 Published online by Cambridge University Press

magnetisation and pressure anisotropy have a destabilising influence on the growth rate of the firehose instability. In the case of strong magnetisation, the growth rate of the firehose instability is increased due to the Ohmic diffusion coefficient. The presence of rotation plays a crucial role in determining the stability of the plasma system. If the rotation exceeds a particular value $\Omega_c = 0.8\ \mathrm{s}^{-1}$ for a white dwarf, then it will be completely stable against the gravitational collapse due to inhomogeneities. For typical white dwarfs, the measured Jeans length $\lambda_{J_1} \simeq 1.8 \times 10^3$ km and Jeans mass $M_{J_1} = 0.04 M_\odot$ point out the possibility of gravitational collapse. More specifically, these results can be applied to understand the gravitational collapse of the hottest known highly magnetised white dwarf RE J0317-853, which has effective temperature $T = 5 \times 10^4$ K and magnetic field $B = 340$ MG (Barstow *et al*. 1995). The strongly magnetised and rapidly rotating systems are more sensitive to firehose instability than weakly magnetised plasmas and slowly rotating systems. The quantum effects, viscosity and centrifugal forces due to rotation help to stabilise the plasma from further collapse due to gravitational instability. The growth of the firehose instability achieves its peak value at a cutoff value of the Alfvén velocity, after which it is completely turned off. The results are interpreted in white dwarfs by measuring the Jeans length, Jeans mass and Jeans frequency and showing the possibility of excitation of the low-frequency CGL waves, firehose instability and gravitational instability in anisotropic quantum plasmas.

It is interesting to note that the density-dependent viscosity in non-Newtonian fluids has a significant impact on the transport properties of complex plasmas (Ivlev *et al*. 2007; Banerjee *et al*. 2013). Thus, in future works, we will consider the role of non-Newtonian viscosity effects on the Jeans instability of isotropic magnetised quantum plasmas.

Acknowledgements

This work is supported by Anusandhan National Research Foundation (ANRF), New Delhi, under core research grant no. CRG/2022/000591. R.P.P. gratefully acknowledges the Inter-University Centre for Astronomy and Astrophysics (IUCAA), Pune, for awarding him a visiting associateship. V.K.S. and R.B. acknowledge the Council of Scientific & Industrial Research (CSIR), New Delhi, for awarding research fellowships. The authors thank the reviewers for providing many fruitful suggestions and constructive comments to improve the manuscript.

Editor Edward Thomas, Jr. thanks the referees for their advice in evaluating this article.

Declaration of interests

The authors have no conflicts to disclose.

Data availability statement

Data sharing is not applicable to this article as no new data were created or analysed in this study.

REFERENCES

ALI, S. & MUSHTAQ, A. 2011 Role of Jeans instability in multi-component quantum plasmas in the presence of Fermi pressure. *Chin. Phys. Lett.* **28**, 075204.

ASENJO, F.A. 2012 The quantum effects of the spin and the Bohm potential in the oblique propagation of magnetosonic waves. *Phys. Lett. A* **376**, 2496–2500.

BANERJEE, D., GARAI, S., JANAKI, M.S. & CHAKRABARTI, N. 2013 Kelvin-Helmholtz instability in non-Newtonian complex plasma. *Phys. Plasmas* **20**, 073702.

BARSTOW, M.A., JORDAN, S., O'DONOGHUE, D., BURLEIGH, M.R., NAPIWOTZKI, R. & HARROP-ALLIN, M.K. 1995 RE J0317 – 853: the hottest known highly magnetic DA white dwarf. *Mon. Not. R. Astron. Soc.* **277**, 971–985.

BHAKTA, S. & PRAJAPATI, R.P. 2018 Effects of Hall current and electrical resistivity on the stability of gravitating anisotropic quantum plasma. *Phys. Plasmas* **25**, 022101.

BOHM, D. 1952 A suggested interpretation of the quantum theory in terms of "Hidden" variables. I. *Phys. Rev.* **85**, 166–179.

BONITZ, M., FILINOV, A., BÖNING, J. & DUFTY, J.W. 2010 *Introduction to Quantum Plasmas*. Berlin, Heidelberg: Springer.

BONITZ, M., MOLDABEKOV, ZH A. & RAMAZANOV, T.S. 2019 Quantum hydrodynamics for plasmas—quo vadis? *Phys. Plasmas* **26**, 090601.

BRAGINSKII, S.I. 1965 Transport processes in a plasma. *Rev. Plasma Phys.* **1**, 205.

BRET, A. 2007 Filamentation instability in a quantum plasma. *Phys. Plasmas* **14**, 084503.

BRODIN, G. & MARKLUND, M. 2007*a* Spin magnetohydrodynamics. *New J. Phys.* **9**, 277–277.

BRODIN, G. & MARKLUND, M. 2007*b* Spin solitons in magnetized pair plasmas. *Phys. Plasmas* **14**, 112107.

BRODIN, G., MARKLUND, M. & MANFREDI, G. 2008 Quantum plasma effects in the classical regime. *Phys. Rev. Lett.* **100**, 175001.

BYCHKOV, V., MODESTOV, M. & MARKLUND, M. 2010 Magnetohydrodynamic instability in plasmas with intrinsic magnetization. *Phys. Plasmas* **17**, 112107.

CHABRIER, G. 1993 Quantum effects in dense Coulombic matter: application to the cooling of white dwarfs. *Astrophys. J.* **414**, 695.

CHEN, S., LI, C., ZHA, X., ZHANG, X. & XIA, Z. 2020 High-frequency surface waves in quantum plasmas with electrons relativistic degenerate and exchange-correlation effects. *Chin. J. Phys.* **68**, 79–86.

DUNCAN, R.C. & THOMPSON, C. 1992 Formation of very strongly magnetized neutron stars: implications for gamma-ray bursts. *Astrophys. J.* **392**, L9.

DURISEN, R.H. 1973 Viscous effects in rapidly rotating stars with application to white-dwarf models. *Theory Techniques. Astrophys. J.* **183**, 205.

EL-TAIBANY, W.F., KARMAKAR, P.K., BESHARA, A.A., EL-BORIE, M.A., GWAILY, S.A. & ATTEYA, A. 2022 Comparison study of the energy and instability of ion-acoustic solitary waves in magnetized electron-positron-ion quantum plasma. *Sci. Rep.* **12**, 19078.

ELSING, D., PÁLFFY, A. & WU, Y. 2022 Quantum effects on plasma screening for thermonuclear reactions in laser-generated plasmas. *Phys. Rev. Res.* **4**, L022004.

FERRARIO, L., VENNES, S., WICKRAMASINGHE, D.T., BAILEY, J.A. & CHRISTIAN, D.J. 1997 EUVE J0317 — 855: a rapidly rotating, high-field magnetic white dwarf. *Mon. Not. R. Astron. Soc.* **292**, 205–217.

FERRARIO, L. & WICKRAMASINGHE, D.T. 2005 Magnetic fields and rotation in white dwarfs and neutron stars. *Mon. Not. R. Astron. Soc.* **356**, 615–620.

GORDON, B.E. & HOLLWEG, J.V. 1983 Collisional damping of surface waves in the solar corona. *Astrophys. J.* **266**, 373.

GÓMEZ, D.O. & KANDUS, A. 2018 Normal modes in magnetized two-fluid spin quantum plasmas. *Mon. Not. R. Astron. Soc.* **481**, 3988–3999.

HAAS, F. 2005 A magnetohydrodynamic model for quantum plasmas. *Phys. Plasmas* **12**, 062117.

HAAS, F. 2008 Quantum Weibel instability. *Phys. Plasmas* **15**, 022104.

HAAS, F. 2011 *Quantum Plasmas: An Hydrodynamic Approach*. New York: Springer.

HAAS, F., MENDONÇA, J.T. & TERÇAS, H. 2023 Plasmon dispersion and Landau damping in the nonlinear quantum regime. *Phys. Rev. E* **108**, 055203.

HAMMAD, A., SHAHZAD, M., SAJJAD, H. & MAHNAZ, H. 2023 Instability and growth rate of magnetosonic waves in quantum plasmas with oblique magnetic field due to coupling of neutrino beam and flavor oscillations. *Eur. Phys. J. Plus* **138**, 784.

HAN, Z., ZHANG, S. & DAI, X. 2019 Charge density waves in a quantum plasma. *Phys. Rev. B* **100**, 155132.

IBEN, I.Jr., TUTUKOV, A.V. & FEDOROVA, A.V. 1998 On the luminosity of white dwarfs in close binaries merging under the influence of gravitational wave radiation. *Astrophys. J.* **503**, 344–349.

IVLEV, A.V., STEINBERG, V., KOMPANEETS, R., HÖFNER, H., SIDORENKO, I. & MORFILL, G.E. 2007 Non-Newtonian viscosity of complex-plasma fluids. *Phys. Rev. Lett.* **98**, 145003.

JAMIL, M., ILYAS, M., RASHEED, A., AYESHA, R., ASIF, M. & SHAHID, M. 2020 Oblique waveguide instability in quantum plasmas. *Phys. Scr.* **95**, 115601.

JAN, Q., MUSHTAQ, A. & IKRAM, M. 2018 Non-linear Alfvén waves in spin-1/2 quantum plasma. *Phys. Plasmas* **25**, 022903.

JOSHI, H., PATIDAR, A.K., SHRIVASTAVA, V. & PENSIA, R.K. 2018 Jeans radiative instability with FLR correction in astrophysical quantum plasma. *Phys. Plasmas* **25**, 022901.

KARPIUK, T., NIKOŁAJUK, M., GAJDA, M. & BREWCZYK, M. 2021 Modelling quantum aspects of disruption of a white dwarf star by a black hole. *Sci. Rep.* **11**, 2286.

KHODACHENKO, M.L., ARBER, T.D., RUCKER, H.O. & HANSLMEIER, A. 2004 Collisional and viscous damping of MHD waves in partially ionized plasmas of the solar atmosphere. *Astron. Astrophys.* **422**, 1073–1084.

KHODADADI AZADBONI, F. 2021 Quantum effects role on the electromagnetic instability growth rate in turbulent state of the fuel fusion. *Chin. J. Phys.* **71**, 375–384.

LEUNG, Y.C. 1985 *Physics of Dense Matter*. Singapore: World Scientific.

LOU, Y.-Q. 1995 Possible oscillation modes of magnetic white dwarfs. *Mon. Not. R. Astron. Soc.* **275**, L11–L15.

LUNDIN, J., MARKLUND, M. & BRODIN, G. 2008 Modified Jeans instability criteria for magnetized systems. *Phys. Plasmas* **7**, 072116.

MAMUN, A.A., SHARMIN, B.E. & TAMANNA, N.K. 2021 Roles of degenerate quantum plasma temperature and stationary heavy nucleus species in nucleus-acoustic shock waves. *Res. Phys.* **29**, 104799.

MANFREDI, G., HERVIEUX, P. & HURST, J. 2021 Fluid descriptions of quantum plasmas. *Rev. Mod. Plasma Phys.* **5**, 7.

MARKLUND, M. & BRODIN, G. 2007 Dynamics of spin- 1/2 quantum plasmas. *Phys. Rev. Lett.* **98**, 025001.

MAROOF, R., MUSHTAQ, A. & QAMAR, A. 2016 Quantum dust magnetosonic waves with spin and exchange correlation effects. *Phys. Plasmas* **23**, 013704.

MARUYAMA, T., BALANTEKIN, A.B., CHEOUN, M.-K., KAJINO, T. & MATHEWS, G.J. 2018 Axion production from landau quantization in the strong magnetic field of magnetars. *Phys. Lett. B* **779**, 160–165.

MODESTOV, M., BYCHKOV, V. & MARKLUND, M. 2009 The Rayleigh–Taylor instability in quantum magnetized plasma with para- and ferromagnetic properties. *Phys. Plasmas* **16**, 032106.

MUSHTAQ, A. & VLADIMIROV, S.V. 2011 Arbitrary magnetosonic solitary waves in spin 1/2 degenerate quantum plasma. *Eur. Phys. J. D* **64**, 419–426.

NEJADTAGHI, F., MAHDAVI, M., HASSANPOUR, S., KHANZADEH, H. & TAVASSOLI, A. 2024 Analytical expression of Weibel electromagnetic instability growth rate in strongly coupled quantum plasma. *Chin. J. Phys.* **89**, 1644–1653.

PELISOLI, I. 2021 Found: a rapidly spinning white dwarf in lamost j024048.51+195226.9. *Mon. Not. R. Astron. Soc.* **509**, L31.

PRAJAPATI, R.P. 2017 Influence of neutrino beam on the Jeans instability in a magnetized quantum plasma. *Phys. Plasmas* **24**, 122902.

RAHIM, Z., ADNAN, M. & QAMAR, A. 2019 Magnetosonic shock waves in magnetized quantum plasma with the evolution of spin-up and spin-down electrons. *Phys. Rev. E* **100**, 053206.

RAPPAZ, Y. & SCHOBER, J. 2024 The effect of pressure-anisotropy-driven kinetic instabilities on magnetic field amplification in galaxy clusters. *Astron. Astrophys.* **683**, A35.

ROGERS, B.N., ZHU, B. & FRANCISQUEZ, M. 2018 Gyrokinetic theory of slab universal modes and the non-existence of the gradient drift coupling (GDC) instability. *Phys. Plasmas* **25**, 052115.

SANGWAN, V.K. & PRAJAPATI, R.P. 2023 Wave modes and instabilities in gravitating magnetized polytropic quantum plasmas including viscosity tensor and FLR corrections. *Mon. Not. R. Astron. Soc.* **525**, 1–11.

SHARMA, K., TURI, J., ALI, R. & DEKA, U. 2024 Modulation instability of magnetosonic waves in semiconducting quantum plasma considering Fermi degenerate pressure, exchange correlation potential, and Bohm potential. *Phys. Fluids* **36**, 074108.

SHARMA, P. & CHHAJLANI, R.K. 2013 The effect of finite Larmor radius corrections on Jeans instability of quantum plasma. *Phys. Plasmas* **20**, 092101.

SHARMA, P. & CHHAJLANI, R.K. 2014 The effect of spin induced magnetization on Jeans instability of viscous and resistive quantum plasma. *Phys. Plasmas* **21**, 032101.

SHUKLA, P., MENDIS, D. & KRASHENINNIKOV, S. 2011 Wave propagation in the magnetized cores of white dwarf stars with ultra-relativistic degenerate electrons. *J. Plasma Phys.* **77**, 571–575.

SHUKLA, P.K. & STENFLO, L. 2006 Jeans instabilities in quantum dusty plasmas. *Phys. Lett. A* **355**, 378–380.

SHUKLA, P.K. & STENFLO, L. 2008 Quantum Hall-MHD equations for a non-uniform dense magnetoplasma with electron temperature anisotropy. *J. Plasma Phys.* **74**, 575–579.

SUTANTYO, W. 1974 On the tidal evolution of massive X-ray binaries. *Astron. Astrophys.* **35**, 251.

TANDON, J.N. & TALWAR, S.P. 1963 Stability of a rotating plasma with anisotropic pressure. *Nucl. Fusion* **3**, 75–77.

TERRERO, D.A., MEDEROS, V.H., PÉREZ, S.L., PARET, D.M., MARTÍNEZ, A.P. & ANGULO, G.Q. 2019 Modeling anisotropic magnetized white dwarfs with γ metric. *Phys. Rev. D* **99**, 023011.

USMAN, S. & MUSHTAQ, A. 2021 Magnetorotational instability in quantum dusty plasma. *Astrophys. J.* **911**, 50.

USMAN, S., MUSHTAQ, A. & JAN, Q. 2018 Magnetorotational instability in spin quantum plasmas. *Phys. Rev. E* **98**, 033202.

WICKRAMASINGHE, D.T. & FERRARIO, L. 2005 The origin of the magnetic fields in white dwarfs. *Mon. Not. R. Astron. Soc.* **356**, 1576–1582.

ZAHN, J.P. 1977 Tidal friction in close binary systems. *Astron. Astrophys.* **57**, 383.